Check for updates

ADVANCED QUANTUM TECHNOLOGIES
www.advquantumtech.com

Efficient Conversion from Atomic Spin Wave to Single Photon with Controllable Temporal Length

*Jiajin Lu, Minjie Wang, Haole Jiao, Mengqi Xi, Zhifang Yang, and Shujing Li**

The single photons with controllable temporal length are essential to connect various heterogeneous nodes in quantum networks. The spontaneous Raman scattering (SRS) process in atomic ensembles is a candidate for generating heralded single photon sources. However, efficient conversion from atomic spin waves to single photons with controllable temporal length has not yet been demonstrated experimentally. Here SRS is used in a cold atomic ensemble to generate Stokes photons, which herald the generation of the correlated atomic spin waves. By applying read pulses with adjustable duration to the atoms, the spin waves are converted to heralded single photons (anti-Stokes photons) with controllable temporal length. The conversion efficiency from atomic spin waves to anti-Stokes photons is improved by utilizing cavity enhancement. The heralded single photons are proved to be nonclassical and to be in a pure state when the photon duration ranges from 100 ns to 3 μs. The conversion efficiency of photons from atomic spin waves is 80 ± 0.5% (63 ± 1.2%) for the anti-Stokes photon duration of 3 μs (100 ns). The research offers an experimental foundation for the interconnection of heterogeneous quantum nodes.

1. Introduction

Quantum networks is one of the important development directions of future information technology,[1] which offers the foundation and platform for large-scale quantum communication[2–4] and distributed quantum computation.[5,6] In quantum networks, single photons carrying information are transmitted in quantum channels to connect quantum nodes.[7–10] Quantum nodes have been developed for a variety of systems, such as individual atoms or ions[5,11,12] solid-state systems,[13,14] and atomic ensembles.[15–19] Different storage media have their own advantages in terms of key parameters for quantum repeater, such as storage lifetime,[20,21] storage efficiency,[22,23] storage bandwidth,[24–27] and storage capacity.[28,29] For combining these advantages in quantum networks, much attention has been devoted to hybrid quantum network with heterogeneous nodes.[30] However, the durations of photon pulses excited or absorbed vary depending on the storage media in quantum nodes, for example, 80 ns for atomic ensemble via Duan–Lukin–Cirac–Zoller (DLCZ) protocol,[31] 700 ns[32] (400 ns[15]) for cold atoms ensemble through electromagnetically induced transparency storage scheme, ≈7 μs for crystals via the atomic frequency combs storage scheme.[33] Therefore, in order to realize the interconnection of heterogeneous nodes, the primary requirement is to prepare the single photons with controllable temporal length.

The generation of single photon sources with controllable temporal length has been demonstrated in atomic ensembles based on spontaneous four-wave mixing [25,34] and DLCZ,[17,35] and also in trapped single ions.[24] The heralded single-photon source generated from atomic ensembles based on DLCZ scheme, has intrinsic storage capability, which facilitates synchronization with other identical sources.[36] By applying read pulses with adjustable durations in atomic memory, Pau Farrera et al. demonstrated a single photon source with a temporal duration tuning range from 10^{-2} to 10 μs based on DLCZ scheme in a cold atomic ensemble.[35] To our knowledge, this work reports the maximum adjustment range of pulse durations for single photons created from atomic ensembles. The high retrieval efficiency is necessary to improve the probability of conversion from atomic spin waves to single photons conditioned on a heralding event. In addition, the retrieval efficiency has a significant effect on the communication rate.[37–40] According to theoretical estimations, a 1% increase in the conversion efficiency can improve the communication rate by 10–14%.[41] Efficient conversion from atomic spin waves to single photons with controllable temporal length has not yet been demonstrated experimentally.

In this work, we present an efficient conversion from atomic spin waves to single photons with controllable temporal length. Based on the DLCZ protocol in a cold atomic ensemble, Stokes photons are emitted with a certain probability when the atomic ensemble is illuminated by write pulses, which heralds the generation of correlated atomic spin waves. Then, by applying read

J. Lu, M. Wang, H. Jiao, M. Xi, Z. Yang, S. Li
The State Key Laboratory of Quantum Optics Technologies and Devices
Institute of Opto-Electronics
Shanxi University
Taiyuan 030006, China
E-mail: lishujing@sxu.edu.cn

J. Lu, M. Wang, H. Jiao, M. Xi, Z. Yang, S. Li
Collaborative Innovation Center of Extreme Optics
Shanxi University
Taiyuan 030006, China

The ORCID identification number(s) for the author(s) of this article can be found under https://doi.org/10.1002/qute.202400480

DOI: 10.1002/qute.202400480

 © 2025 Wiley-VCH GmbH

pulses, the spin waves are converted to heralded single photons (anti-Stokes photons) correlated with Stokes photons. A medium-finesse ring cavity is placed around the atomic ensemble to improve the conversion efficiency. By changing the read pulse duration, we realize the controllable adjustment of the anti-Stokes photon duration. For the anti-Stokes photon duration of 25 μs (100 ns), the cross-correlation function $g^{(2)}_{S,aS} = 2.3 \pm 0.29$ ($g^{(2)}_{S,aS} = 26.5 \pm 0.4$) with a retrieval efficiency of $80.07 \pm 0.2\%$ ($63 \pm 1.2\%$). When the anti-Stokes photon duration ranges from 100 ns to 3 μs, the heralded autocorrelation function of anti-Stokes photons $\alpha_{D_1,D_2|D_S}$ remains below the classical bound of 1, and the measurement of the unheralded autocorrelation function of anti-Stokes photons α_{D_1,D_2} shows that the anti-Stokes photons are emitted in a pure state. In addition, by employing the magnetic-field-insensitive states to store the atomic SWs and the collinear configuration, the atomic memory lifetime reaches 0.4 ms, in which the synchronization of two single-photon sources may be achieved.[36] This work enriches the toolbox of hybrid quantum information technology.

2. Experimental Setup

The experimental setup is shown in **Figure 1a**. A cold ^{87}Rb atomic cloud prepared in a magneto-optical trap serves as the memory medium. We apply a biased magnetic field ($B_0 = 4$G) to the atomic cloud to define the quantization axis (Z axis). The relevant energy levels are shown in Figure 1b, where $|g\rangle = |5S_{1/2}, F = 1\rangle$, $|s\rangle = |5S_{1/2}, F = 2\rangle$, $|e_1\rangle = |5P_{1/2}, F' = 1\rangle$ and $|e_2\rangle = |5P_{1/2}, F' = 2\rangle$. The atoms are initially prepared to $|g, m_F = 0\rangle$ by optical pumping. To achieve a high retrieval efficiency, a ring cavity is employed to increase the effective optical depth (OD). The cavity length is ≈5.5 m and the finesse is 15 with a linewidth of 3.7 MHz. The ring cavity consists of three highly reflecting mirrors (HR_1, HR_2, and HR_3), and an output coupler (OC) with reflectivity of 80%. Two optical lenses L_1 and L_2 are symmetrically placed on both sides of the atomic ensemble to ensure that the waist of the cavity mode is positioned at the atomic ensemble.

A Gaussian-shaped write pulse of 50 ns duration (full-width at half-maximum, FWHM), red-detuned from the $|5S_{1/2}, F = 1\rangle \rightarrow |5P_{1/2}, F' = 1\rangle$ transition by 60 MHz, is applied to the atomic ensemble to generate the pairs of Stokes photons and spin waves by SRS. The σ^+-polarized write pulse intersects with the cavity mode through the atomic ensemble with an angle of 0.15°. The emitted Stokes photons propagating clockwise along the cavity mode are collected. During the writing process, both the σ^+- and σ^--polarized Stokes fields may be excited. When a σ^+ (σ^-)-polarized Stokes photon is emitted, a corresponding magnetic-field-insensitive (magnetic-field-sensitive) spin-wave (SW) is stored in the atomic ensemble, which is associated with the coherence $|g, m_F = 0\rangle \leftrightarrow |s, m_F = 0\rangle$ ($|g, m_F = 0\rangle \leftrightarrow |s, m_F = 2\rangle$). After a quarter wave plate QWs and a half wave plate HWs, the σ^+-polarized Stokes field becomes vertically (V) polarized. The field can keep its propagation direction passing through a beam displacer BD and resonate with the cavity mode. However, after QWs and HWs the emitted σ^--polarized Stokes photon becomes horizontally (H) polarized, which will be deviated from the cavity mode by BD and blocked, as shown in Figure 1a. We use BD to remove the σ^--polarized photons from the Stokes field, leaving only the σ^+-polarized photons. In this way, the magnetic-sensitive SW of atomic memory is eliminated, which is beneficial for improving the memory lifetime.

After the σ^+-polarized Stokes photon escapes out of the cavity from OC, it is directed to the single photon detector D_S. Conditioned on the detection of a Stokes photon, the generation of the atomic SW is heralded. The SW stored in the atomic ensemble can be described as:[35]

$$|1_s\rangle = \frac{1}{\sqrt{N}} \sum_{j=1}^{N} e^{ix_j \cdot \Delta k} |g_1 \ldots s_j \ldots g_N\rangle \quad (1)$$

where N is the number of atoms, x_j denotes the spatial position of the jth atom, $\Delta k = k_W - k_S$ is the wave vector of the SW, k_W and k_S are the wave vectors of write beam and Stokes field, respectively. The joint state of the Stokes photon and the associated SW is described by the two-mode compressed state:

$$|\phi\rangle = \sqrt{1-p}\left(|0_w\rangle |0_s\rangle + \sqrt{p}\,|1_w\rangle |1_s\rangle + p\,|2_w\rangle |2_s\rangle + o\left(p^{3/2}\right)\right) \quad (2)$$

where p is the probability to create a SW correlated with a Stokes photon in the detection mode.

After a storage time t, the read pulse counter-propagating with the write pulse, which is red-detuned from the $|5S_{1/2}, F = 2\rangle \rightarrow |5P_{1/2}, F' = 2\rangle$ transition by 110 MHz, converts the SW into a σ^+-polarized anti-Stokes filed. The anti-Stokes field becomes V-polarized after a quarter wave plate QW_{aS} and a half wave plate HW_{aS}. It propagates counterclockwise in the cavity and is also resonant with the cavity.

To realize the simultaneous resonance of the Stokes and anti-Stokes fields with the cavity, a locking beam is coupled to the cavity from the OC by a beam splitter BS with reflectivity of 1%. The locking beam is red-detuned from the $|5S_{1/2}, F = 2\rangle \rightarrow |5P_{1/2}, F' = 2\rangle$ transition by 230 MHz, which is far-detuned from the Stokes photons and anti-Stokes photons. By varying the position of the cavity mirror HR_3 mounted on a manual translation stage, we find a cavity length to achieve the simultaneous resonance of the Stokes field, anti-Stokes field, and the locking beam with the cavity. The cavity length is locked by implementing the Pound–Drever–Hall (PDH) method to the locking beam. The anti-Stokes field is detected by single photon detector D_{aS} after escaping out of the cavity from OC. We place an optical-spectrum-filter set (OSFS) before detectors D_S and D_{aS}, respectively, to suppress noise from the leakage from write, read, and locking beams.

The experiment period is 50 ms, of which 42 ms is used for loading the atoms and the next 8 ms is for generating the atom-photon quantum interfaces, as shown in Figure 1c. A field-programmable gate array (FPGA) is used to generate timing control signals and perform single-photon signal acquisition. Initially, the atoms are prepared for the state $|g, m_F = 0\rangle$ through an optical pumping process. Then the write pulse is applied to the atoms and the detection of the Stokes photon is recorded. If no Stokes photons are detected, the pumping pulses are applied to prepare the atoms back to the initial state, and then the next trial starts. Conditioned on a detection event, the corresponding SW is generated, and the FPGA sends out a feed-forward signal to stop the write processes.[42] After a storage time t, a read pulse

© 2025 Wiley-VCH GmbH

25119044, 0, Downloaded from https://onlinelibrary.wiley.com/doi/10.1002/qute.202400480 by Shu-Jing Li - Shanxi University , Wiley Online Library on [12/02/2025]. See the Terms and Conditions (https://onlinelibrary.wiley.com/terms-and-conditions) on Wiley Online Library for rules of use; OA articles are governed by the applicable Creative Commons License

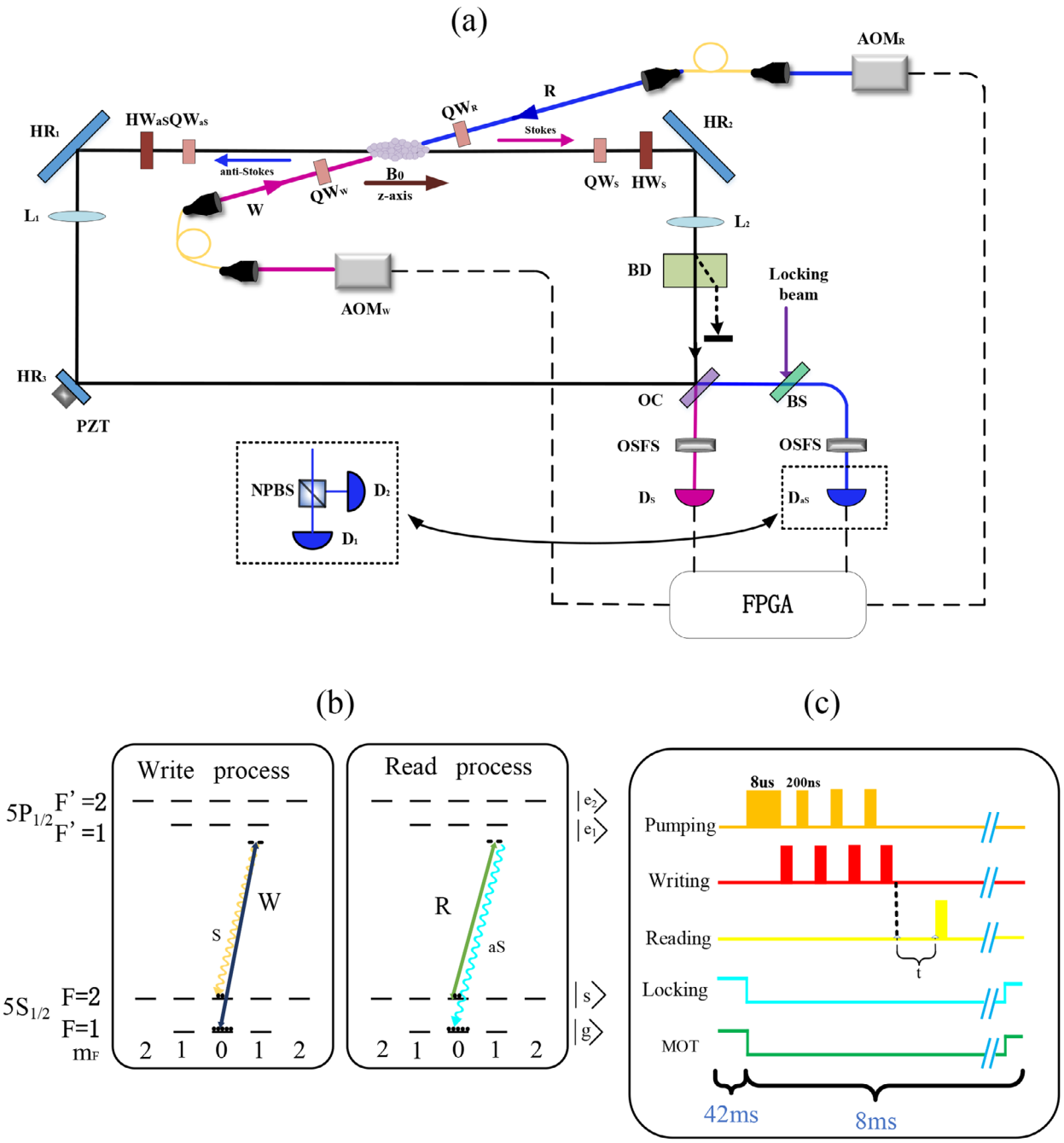

Figure 1. Overview of the experiment. a) Setup for the experiment. HR_1, HR_2, and HR_3: highly reflecting mirrors; PZT: piezoelectric transducer; L1, L2: lens; BD: beam displacer; $HW_{S(aS)}$: half wave plate in the Stokes (anti-Stokes) channel; $QW_{S(aS)}$: quarter wave plate in the Stokes (anti-Stokes) channel; $AOM_{W(R)}$: acousto-optic modulator to generate the writing (reading) pulse; OC: output coupler; BS: beam splitters; OSFS: optical-spectrum-filter set; PBS: polarizing beam splitter; $D_{S(aS)}$: Single photon detector for Stokes (anti-Stokes) photons. The set-up depicted in the region enclosed by the dotted rectangle on the left is used to measure the autocorrelation function. NPBS: non-polarization beam splitter. $D_{1(2)}$: Single photon detector. b) Relevant energy levels involved in the writing and reading process. W(R) represents the writing (reading) field, S(aS) represents the σ^+-polarized Stokes (anti-Stokes) photons. c) Time sequence for the experimental trials.

with a controllable duration τ_R is applied to the atomic ensemble to convert the SW into an anti-Stokes photon. The width of the acquisition window for anti-Stokes photons needs to be adjusted as the duration of the read pulse.

3. Experimental Section

The influence of the reading pulse duration τ_R was first measured on the anti-Stokes photons duration τ_{aS}. By driving the acousto-optic modulator AOM_R (Gooch&Housego 3200-124) with an arbitrary waveform gen-

© 2025 Wiley-VCH GmbH

25119044, 0, Downloaded from https://onlinelibrary.wiley.com/doi/10.1002/qute.202400480 by Shu-Jing Li - Shanxi University , Wiley Online Library on [12/02/2025]. See the Terms and Conditions (https://onlinelibrary.wiley.com/terms-and-conditions) on Wiley Online Library for rules of use; OA articles are governed by the applicable Creative Commons License

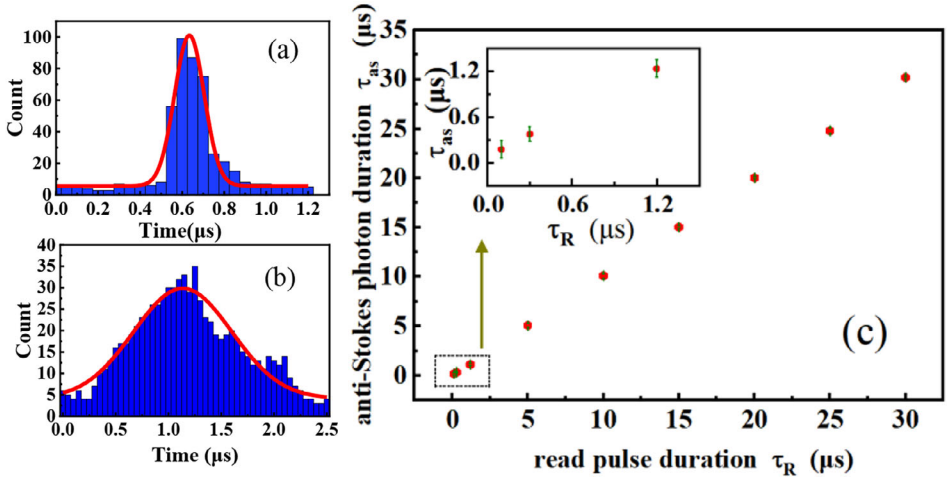

Figure 2. a,b) are the measured anti-Stokes photon wave shape (blue histograms) when the read pulse is 100 ns and 1 μs, respectively. c) Temporal duration of the anti-Stokes photon (FWHM) versus the duration of the read pulse. The inset of (c) shows the details of the anti-Stokes photon duration when the read pulse is less than 2 μs.

erator (Tektronix AFG-3252), the Gaussian-shaped read pulses of variable durations (FWHM) were generated. The wave shapes of anti-Stokes photons were measured for the reading pulses with different durations. **Figure 2**a,b are two examples of the wave shapes of anti-Stokes photons for $\tau_R = 100$ ns and $\tau_R = 1$ μs, respectively. The wave shape of the anti-Stokes photon was also Gaussian-shaped and the duration was $\tau_{aS} = 175$ ns ($\tau_{aS} = 1.01$ μs) for $\tau_R = 100$ ns ($\tau_R = 1$ μs). The anti-Stokes photons' duration τ_{aS} was shown as a function of the reading pulse duration τ_R in Figure 2c. For $\tau_R > 1$μs, $\tau_{aS} = \tau_R$, which reflects that the duration of the reading pulse could be transferred to the anti-Stokes photons. For τ_R ranges from 100 ns to 1 μs, the wave shape of the anti-Stokes photon was widened in the time domain because of the narrow linewidth of the cavity (3.7 MHz). By increasing the linewidth of the cavity, the wave shape of the reading pulse with a shorter duration can be transferred to the anti-Stokes photon.

Then, the intrinsic retrieval efficiency γ was measured as the function of the anti-Stokes photon duration τ_{aS}, as shown in **Figure 3**. The retrieval efficiency was defined as $\gamma = P_{S,aS}/\eta_{D_{aS}} P_S$, where $P_S(P_{aS})$ was the detection probability for Stokes (anti-Stokes) photons by detector D_S (D_{aS}), $P_{S,aS}$ was the coincidence probability between D_S and D_{aS}, and $\eta_{D_{aS}} = 0.14$ was the overall detection efficiency of the anti-Stokes photon including

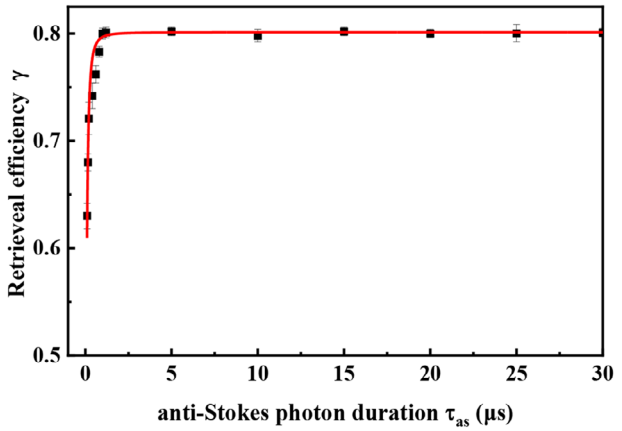

Figure 3. Retrieval efficiency as a function of the photon duration τ_{aS} at the zero delay with an excitation probability of $\chi \approx 1.5\%$. The data are fitted according to Equation (6), as shown by the red line, which yields $k \cdot D \cdot E_0 = 4.03$.

escaping efficiency from the cavity ($\eta_e \approx 0.55$), the transmission of the anti-Stokes photon channel ($\eta_T \approx 0.37$) and the detection efficiency of D_{aS} ($\eta_D \approx 0.68$). The experimental results show the retrieval efficiency γ increases with the anti-Stokes photon duration τ_{aS} and γ reaches 80% and becomes saturated for $\tau_{aS} > 1$ μs.

A simple theoretical model was developed to describe the relation between the intrinsic retrieval efficiency γ and the anti-Stokes photon duration τ_{aS}. The normalized frequency spectrum of Gauss-shaped anti-Stokes photon pulse can be described as:

$$S_{aS} = \frac{1}{\sqrt{2\pi}\sigma_{aS}} \exp\left[-\frac{(f-f_0)^2}{2\sigma_{aS}^2}\right] \tag{3}$$

where f_0 is the central frequency of anti-Stokes photon, $\sigma_{aS} = \frac{\sqrt{2\ln 2}}{\pi W_{aS}^t}$, and W_{aS}^t is the FWHM of the anti-Stokes photon pulse in the time domain. A Gaussian function was used to approximate the frequency spectrum of the cavity, which can be written as:

$$S_C = E_0 \exp\left[-\frac{(f-f_0)^2}{2\sigma_C^2}\right] \tag{4}$$

where E_0 represents the enhancement factor resonating with the cavity, f_0 is the resonant frequency of the cavity that equals the central frequency of anti-Stokes photon, $\sigma_C = \frac{W_C^f}{2\sqrt{2\ln 2}}$, and W_C^f is the FWHM of frequency spectrum of the cavity. During the read process, the cavity can enhance the emission of anti-Stokes photons into the cavity mode by a factor of:

$$E = \int_{-\infty}^{+\infty} S_{aS}(f)\, S_C(f)\, df \tag{5}$$

So, the intrinsic retrieval efficiency with the cavity can be expressed as:

$$\gamma = \frac{k\cdot D\cdot E}{k\cdot D\cdot E+1} = \frac{k\cdot D\cdot E_0}{k\cdot D\cdot E_0+\sqrt{1+\left(\frac{4Ln2}{\pi}\right)^2\left(\frac{1}{W_{aS}^t W_C^f}\right)^2}} \tag{6}$$

where k is related to the atomic energy lever, and D is the optical depth of atomic ensemble.

© 2025 Wiley-VCH GmbH

25119044, 0, Downloaded from https://onlinelibrary.wiley.com/doi/10.1002/qute.202400480 by Shu-Jing Li - Shanxi University , Wiley Online Library on [12/02/2025]. See the Terms and Conditions (https://onlinelibrary.wiley.com/terms-and-conditions) on Wiley Online Library for rules of use; OA articles are governed by the applicable Creative Commons License

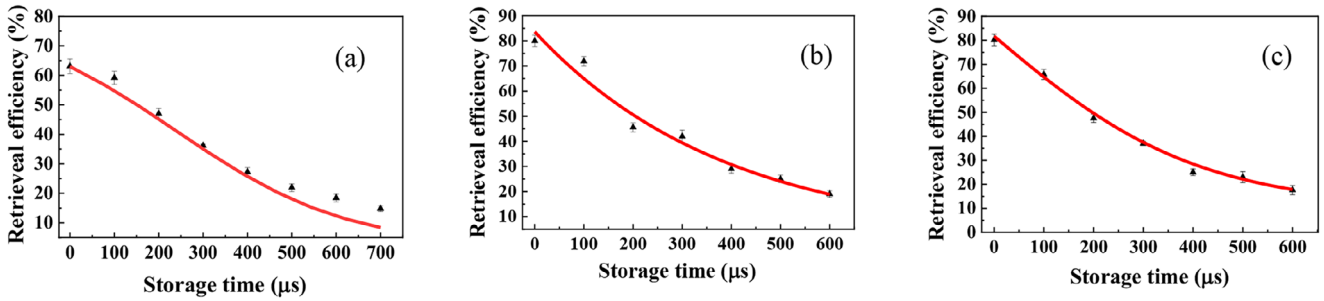

Figure 4. Retrieval efficiency as a function of the storage time t with an excitation probability of $\chi \approx 1.5\%$. The anti-Stokes photon duration in a) 100 ns b) 1 μs, c) 30 μs, respectively.

The experimental data were fit according to Equation (6), as shown by the red line in Figure 3. The theoretical predictions were in good agreement with the experimental data. The reduction of retrieval efficiency for $\tau_{aS} < 1$ μs comes from the imperfect cavity enhancement in the reading process, in which the linewidth of anti-Stokes photon was close to, or even wider than that of the cavity. The retrieval efficiency remains above 60% even though when the anti-Stokes photon duration was reduced to 100 ns. One can increase the cavity linewidth to improve the retrieval efficiency for the anti-Stokes photon with a shorter duration.

Next, the storage lifetime was measured of the SWs for different anti-Stokes photon duration. **Figure 4** shows the retrieval efficiency as a function of the storage time t. The function $\gamma(t) = \frac{\gamma_0}{2}(e^{-(t/t_0)^2} + e^{-t/t_0})$ was used to fit the experimental data, which yields the initial retrieval efficiencies of γ_0= 63.1%, 80%, and 80.1% and the 1/e storage lifetimes of t_0 = 0.43, 0.41, and 0.4 ms for the anti-Stokes photon with durations of 100 ns, 1 μs, and 30 μs.

To characterize the quantum correlation between the Stokes and anti-Stokes photons, the cross-correlation function $g_{S,aS} = P_{S,aS}/P_S \cdot P_{aS}$ was measured, as shown in **Figure 5**. For τ_{aS} = 100 ns, the measured $g_{S,aS}$ was 26.5 ± 0.4. The value $g_{S,aS}$ decreases with the increase of the anti-Stokes photon duration τ_{aS}. In the range of $\tau_{aS} < 25$ μs, the value $g_{S,aS}$ can be maintained above 2. The cross-correlation function $g_{S,aS}$ can be expressed as:

$$g_{S,aS} = 1 + \frac{\gamma(\tau_{aS})}{(B+\chi)\gamma(\tau_{aS}) + f_1\xi(B+\chi)(1-\gamma(\tau_{aS})) + C(\tau_{aS})} \quad (7)$$

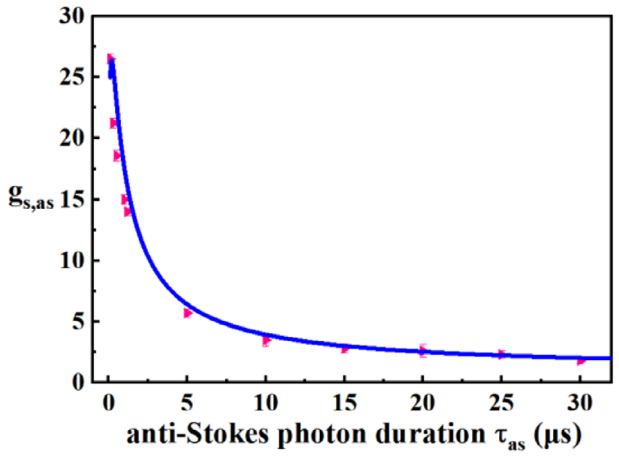

Figure 5. The measured cross-correlation function $g_{S,aS}$ as a function of the anti-Stokes photon duration τ_{aS} at the zero delay with an excitation of $\chi \approx 2\%$. The solid line is the fitting result, where ξ= 0.3 and $C(\tau_{aS}) = 2.5 \times 10^{-2}\tau_{aS}$.

where ξ is the branching ratio corresponding to the anti-Stokes photon transition,[43] $\gamma(\tau_{aS})$ is the duration-dependent retrieval efficiency, $f_1 = \frac{2F}{\pi}$ is the cavity enhancement factor for the nondirectional emission noise, F is the finesse of the cavity, $B = 4 \times 10^{-4}$ denotes the background noise probability in the Stokes photon detection channel, and $C(\tau_{aS})$ is the background noise probability in the anti-Stokes photon detection channel which is proportional to the width of the acquisition window τ_{aS}. The experimental data were fit in Figure 5. according to Equation (7). The experimental and theoretical results were in good agreement. In the fitting, the retrieval efficiency $\gamma(\tau_{aS})$ was taken from the fitting function in Figure 3. As the photon duration τ_{aS} increases, this detection window was extended accordingly, which makes more background noise mix into the anti-Stokes photon detection channel and leads to a decrease in $g_{S,aS}$. To achieve good cross-correlation with a larger anti-Stokes photon duration the noise was required to reduce. The goal could be achieved by using a higher signal-to-noise ratio filter system[44] or choosing low-noise single-photon detectors.

To qualify the anti-Stokes photons as a single-photon source, the heralded autocorrelation function $\alpha_{D_1,D_2|D_S}$ was measured with a Hanbury–Brown–Twiss setup. $\alpha_{D_1,D_2|D_S} = 0$ corresponds to an ideal single photon and $\alpha_{D_1,D_2|D_S} = 1$ corresponds to the classical light. Detection of the Stokes field in detector Ds was used as a trigger, and the anti-Stokes field was split into two fields S_{aS1} and S_{aS2} at a 50:50 non-polarization beam splitter and detected by detectors D_1 and D_2, as shown in the setup depicted in the region enclosed by the dotted rectangle on the left in Figure 1a. The autocorrelation function can be obtained by:

$$\alpha_{D_1,D_2|D_S} = \frac{P_{D_1,D_2|D_S}}{P_{D_1|D_S} \cdot P_{D_2|D_S}} \quad (8)$$

where $P_{D_1|D_S}$ ($P_{D_2|D_S}$) refers to the probability of detecting an anti-Stokes photon via D_1 or D_2 conditioned on a Stokes photon detection. $P_{D_1,D_2|D_S}$ refers to the probability to measure a coincidence between both anti-Stokes photon detections via D_1 and D_2 conditioned on a Stokes photon detection.

Figure 6 shows the heralded autocorrelation function of anti-Stokes field $\alpha_{D_1,D_2|D_S}$ in terms of the anti-stokes photon duration τ_{aS}. For an ideal single photon state, the autocorrelation function should be 0. In the experiment, the measured autocorrelation function was 0.17 ± 0.05 at $\tau_{aS} = 100ns$ due to the multiphoton state and imperfect retrieval efficiency in the DLCZ process. As the anti-Stokes photon duration increases, the detection window also needs to be broadened and more background noise was introduced in the detection process, which destroys the anti-bunching of single photons and the autocorrelation function would soon rise to the classical bound of $\alpha_{D_1,D_2|D_S} = 1$ at $\tau_{aS} = 3.5\mu s$ After this point, the autocorrelation function continues to slowly increase, reaching $\alpha_{D_1,D_2|D_S} = 1.7 \pm 0.05$ at $\tau_{aS} = 30\mu s$. For anti-Stokes photons with long durations, the background noise dominates, and the measured autocorrelation function of anti-Stokes photons was determined by that of the background noise. In the experiment, the background noise in the anti-Stokes photon detection channel was mainly caused by the dark counts of the single-photon

© 2025 Wiley-VCH GmbH

25119044, 0, Downloaded from https://onlinelibrary.wiley.com/doi/10.1002/qute.202400480 by Shu-Jing Li - Shanxi University , Wiley Online Library on [12/02/2025]. See the Terms and Conditions (https://onlinelibrary.wiley.com/terms-and-conditions) on Wiley Online Library for rules of use; OA articles are governed by the applicable Creative Commons License

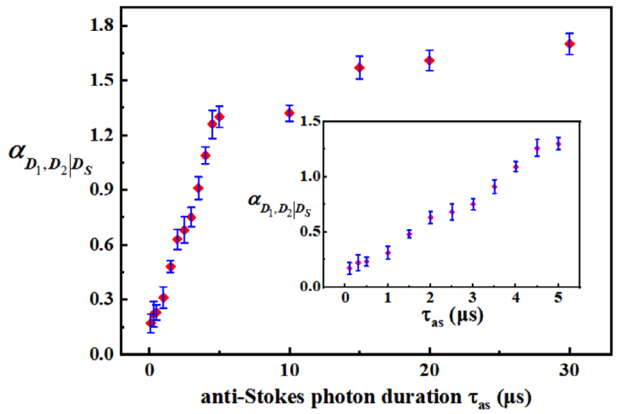

Figure 6. The measured autocorrelation function $\alpha_{D_1,D_2|D_S}$ in terms of the anti-Stokes photon duration τ_{aS} at the zero delay with an excitation of $\chi \approx 2\%$. The inset shows the details of the autocorrelation function when the anti-Stokes photon duration is less than 5 μs.

detectors and the leakage of the reading beam and the beam for the locking cavity. Both the two beams were from semiconductor laser amplifier BoosTAs (Toptica Photonics AG), they include a coherent field at the injection frequency together with a wide noise spectrum. The intensity at the main frequency peak was suppressed by ≈10 orders of magnitude by multiple Fabry–Perot etalons in the detection channel. Thus, the wide noise spectrum dominates, which makes the measured autocorrelation function of anti-Stokes photons with long duration greater than 1.

To characterize the single mode nature of the anti-Stokes photons, the unconditional autocorrelation function $\alpha_{D1,D2}$ was measured. The unheralded autocorrelation function of the anti-Stokes photons could be obtained by $\alpha_{D_1,D_2} = \frac{P_{D_1,D_2}}{P_{D_1} \cdot P_{D_2}}$, where P_{D_1} (P_{D_2}) was the detection probability for anti-Stokes photons by detector D_1 (D_2), and P_{D_1,D_2} was the coincidence probability between D_1 and D_2. **Figure 7** shows the unheralded autocorrelation functions α_{D_1,D_2} as a function of anti-Stokes photon duration τ_{aS}. For the duration of $\tau_{aS} = 100ns$, the unheralded autocorrelation function $\alpha_{D_1,D_2} = 1.83 \pm 0.04$, which was close to 2 corresponding to the ideal two-mode squeezed state with single mode. The unheralded autocorrelation function α_{D_1,D_2} decreases with the increase of τ_{aS}, and $\alpha_{D_1,D_2} = 1.02 \pm 0.04$ at $\tau_{aS} = 5\mu s$. The red line shows the theoretical prediction with a single mode accounting for the background noise in the detection channel. The experimental data were in good agreement with the theoretical prediction. For comparison, the unheralded autocorrelation function was also plotted with two modes, as shown by the dashed purple line. The measured data points were above the theoretical results with two modes in the range of $100ns < \tau_{aS} < 3\mu s$, which confirms the single-mode nature of the emitted anti-Stokes photons.

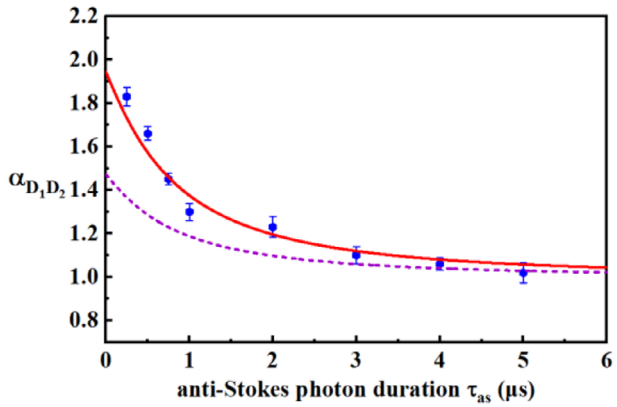

Figure 7. The measurement of unheralded autocorrelation functions $\alpha_{D1,D2}$ as a function of anti-Stokes photon duration τ_{aS} at the zero delay with an excitation of $\chi \approx 2\%$. The red line is a theoretical fitting accounting for the noise probability of detection channel $5 \times 10^{-3}\tau_{aS}$. The dashed purple line represents the theoretical prediction with two modes.

4. Conclusion

We demonstrate an efficient conversion from atomic spin waves to single photons with controllable temporal length. We use SRS to generate the correlated Stokes photons and atomic spin waves in a cold atomic ensemble. By applying read pulses with adjustable duration to the atoms, the spin waves can be converted to heralded single photons (anti-Stokes photons) with controllable temporal length. The cavity enhancement is employed to improve the conversion efficiency. The conversion efficiency reaches 80% for $\tau_{aS} > 1$ μs, and the conversion efficiency can achieve $63 \pm 1.2\%$ even at $\tau_{aS} = 100$ ns. To expand the pulse duration of anti-Stokes photons while maintaining high retrieval efficiency, one can increase the cavity linewidth and reduce the noise in the detection channel of anti-Stokes photons. To quantify the quantum correlation between Stokes and anti-Stokes photons, we measure the cross-correlation function $g^{(2)}_{S,aS}$, which shows that $g^{(2)}_{S,aS} = 2.3 \pm 0.29$ ($g^{(2)}_{S,aS} = 26.5 \pm 0.4$) at $\tau_{aS} = 25$ μs ($\tau_{aS} = 100$ ns). By measuring the heralded and unheralded autocorrelation function of the anti-Stokes photons, it is proved that the anti-Stokes photons are nonclassical and in a pure state when the photon duration ranges from 100 ns to 3 μs.

Here, by using the magnetic-field-insensitive SW, the storage lifetime is prolonged to 0.4 ms, which benefits the synchronization between two identical single photon sources. In our experiment, the single-photon source is heralded with a probability of $P_w = 0.36\%$, which includes the excitation probability of 1% and the whole detection efficiency of Stokes photon 24%. We can generate 104 trials in an 8 ms experiment period for a read pulse length of 300 ns. It can be deduced that the average time separation between heralding events is 0.36 ms, which is less than the storage lifetime of 0.4 ms. The long storage lifetime provides the possibility for synchronization of single photon sources. The research offers an experimental foundation for the interconnection of heterogeneous quantum nodes.

Acknowledgements

This work is supported by the National Natural Science Foundation of China (12174235), the Fund for Shanxi Key Subjects Construction (1331), and the Fundamental Research Program of Shanxi Province (202203021221011)

Conflict of Interest

The authors declare no conflict of interest.

Data Availability Statement

The data that support the findings of this study are available from the corresponding author upon reasonable request.

© 2025 Wiley-VCH GmbH

25119044, 0, Downloaded from https://onlinelibrary.wiley.com/doi/10.1002/qute.202400480 by Shu-Jing Li - Shanxi University , Wiley Online Library on [12/02/2025]. See the Terms and Conditions (https://onlinelibrary.wiley.com/terms-and-conditions) on Wiley Online Library for rules of use; OA articles are governed by the applicable Creative Commons License

Keywords

controllable temporal length, conversion efficiency, heralded single photons, heterogeneous quantum networks

Received: September 26, 2024
Revised: January 20, 2025
Published online:

[1] H. J. Kimble, *Nature* **2008**, *453*, 1023.
[2] C. Simon, *Nat. Photon.* **2017**, *11*, 678.
[3] S. H. Wei, B. Jing, X. Y. Zhang, J. Y. Liao, C. Z. Yuan, B. Y. Fan, C. Lyu, D. L. Zhou, Y. Wang, G. W. Deng, H. Z. Song, D. Oblak, G. C. Guo, Q. Zhou, *Laser Photon. Rev.* **2022**, *16*, 2100219.
[4] L.-M. Duan, M. D. Lukin, J. I. Cirac, P. Zoller, *Nature* **2001**, *414*, 413.
[5] A. Reiserer, G. Rempe, *Rev. Mod. Phys.* **2015**, *87*, 1379.
[6] S. W. S. L. Severin Daiss, E. Distante, P. Thomas, L. Hartung, O. Morin, G. Remp, *Science* **2021**, *371*, 614.
[7] C. W. Chou, S. V. Polyakov, A. Kuzmich, H. J. Kimble, *Phys. Rev. Lett.* **2004**, *92*, 213601.
[8] T. E. Northup, R. Blatt, *Nat. Photon.* **2014**, *8*, 356.
[9] T. Chaneliere, D. N. Matsukevich, S. D. Jenkins, S. Y. Lan, T. A. Kennedy, A. Kuzmich, *Nature* **2005**, *438*, 833.
[10] W. Chang, C. Li, Y. K. Wu, N. Jiang, S. Zhang, Y. F. Pu, X. Y. Chang, L. M. Duan, *Phys. Rev. X.* **2019**, *9*, 041003.
[11] H. P. Specht, C. Nolleke, A. Reiserer, M. Uphoff, E. Figueroa, S. Ritter, G. Rempe, *Nature* **2011**, *473*, 190.
[12] S. Ritter, C. Nolleke, C. Hahn, A. Reiserer, A. Neuzner, M. Uphoff, M. Mucke, E. Figueroa, J. Bochmann, G. Rempe, *Nature* **2012**, *484*, 195.
[13] J. Fekete, D. Rieländer, M. Cristiani, H. de Riedmatten, *Phys. Rev. Lett.* **2013**, *110*, 220502.
[14] K. R. Ferguson, S. E. Beavan, J. J. Longdell, M. J. Sellars, *Phys. Rev. Lett.* **2016**, *117*, 020501.
[15] P. Vernaz-Gris, K. Huang, M. Cao, A. S. Sheremet, J. Laurat, *Nat. Commun.* **2018**, *9*, 363.
[16] Z. Yan, L. Wu, X. Jia, Y. Liu, R. Deng, S. Li, H. Wang, C. Xie, K. Peng, *Nat. Commun.* **2017**, *8*, 718.
[17] X.-H. Bao, A. Reingruber, P. Dietrich, J. Rui, A. Dück, T. Strassel, L. Li, N.-L. Liu, B. Zhao, J.-W. Pan, *Nat. Phys.* **2012**, *8*, 517.
[18] C. Wang, Y. Yu, Y. Chen, M. Cao, J. Wang, X. Yang, S. Qiu, D. Wei, H. Gao, F. Li, *Quantum Science Technol.* **2021**, *6*, 045008.
[19] L. Jiang, J. M. Taylor, M. D. Lukin, *Phy. Rev. A.* **2007**, *76*, 012301.
[20] K. B. Dideriksen, R. Schmieg, M. Zugenmaier, E. S. Polzik, *Nat. Commun.* **2021**, *12*, 3699.
[21] C. Laplane, P. Jobez, J. Etesse, N. Gisin, M. Afzelius, *Phys. Rev. Lett.* **2017**, *118*, 210501.
[22] M. Cao, F. Hoffet, S. Qiu, A. S. Sheremet, J. Laurat, *Optica.* **2020**, *7*, 1440.
[23] Y. W. Cho, G. T. Campbell, J. L. Everett, J. Bernu, D. B. Higginbottom, M. T. Cao, J. Geng, N. P. Robins, P. K. Lam, B. C. Buchler, *Optica* **2016**, *3*, 100.
[24] M. Almendros, J. Huwer, N. Piro, F. Rohde, C. Schuck, M. Hennrich, F. Dubin, J. Eschner, *Phys. Rev. Lett.* **2009**, *103*, 213601.
[25] S. Du, P. Kolchin, C. Belthangady, G. Y. Yin, S. E. Harris, *Phys. Rev. Lett.* **2008**, *100*, 183603.
[26] X. H. Bao, Y. Qian, J. Yang, H. Zhang, Z. B. Chen, T. Yang, J. W. Pan, *Phys. Rev. Lett.* **2008**, *101*, 190501.
[27] D. Lago-Rivera, J. V. Rakonjac, S. Grandi, H. d. Riedmatten, *Nat. Commun.* **2023**, *14*, 1889.
[28] X. Liu, J. Hu, Z. F. Li, X. Li, P. Y. Li, P. J. Liang, Z. Q. Zhou, C. F. Li, G. C. Guo, *Nature* **2021**, *594*, 41.
[29] Y. F. Pu, N. Jiang, W. Chang, H. X. Yang, C. Li, L. M. Duan, *Nat. Commun.* **2017**, *8*, 15359.
[30] M. Wallquist, K. Hammerer, P. Rabl, M. Lukin, P. Zoller, *Phy. Scripta.* **2009**, *T137*, 014001.
[31] S. J. Yang, X. J. Wang, J. Li, J. Rui, X. H. Bao, J. W. Pan, *Phys. Rev. Lett.* **2015**, *114*, 210501.
[32] Y. Wang, J. Li, S. Zhang, K. Su, Y. Zhou, K. Liao, S. Du, H. Yan, S.-L. Zhu, *Nat. Photonics.* **2019**, *13*, 346.
[33] A. Holzäpfel, J. Etesse, K. T. Kaczmarek, A. Tiranov, N. Gisin, M. Afzelius, *New J. Phys.* **2020**, *22*, 063009.
[34] K. Liao, H. Yan, J. He, S. Du, Z. M. Zhang, S. L. Zhu, *Phys. Rev. Lett.* **2014**, *112*, 243602.
[35] P. Farrera, G. Heinze, B. Albrecht, M. Ho, M. Chávez, C. Teo, N. Sangouard, H. de Riedmatten, *Nat. Commun.* **2016**, *7*, 13556.
[36] Y.-F. Pu, S. Zhang, Y.-K. Wu, N. Jiang, W. Chang, C. Li, L.-M. Duan, *Nat. Photonics.* **2021**, *15*, 374.
[37] Y. Yu, F. Ma, X. Y. Luo, B. Jing, P. F. Sun, R. Z. Fang, C. W. Yang, H. Liu, M. Y. Zheng, X. P. Xie, W. J. Zhang, L. X. You, Z. Wang, T. Y. Chen, Q. Zhang, X. H. Bao, J. W. Pan, *Nature* **2020**, *578*, 240.
[38] K. Azuma, S. E. Economou, D. Elkouss, P. Hilaire, L. Jiang, H.-K. Lo, I. Tzitrin, *Rev. Mod. Phys.* **2023**, *95*, 045006.
[39] A. G. Radnaev, Y. O. Dudin, R. Zhao, H. H. Jen, S. D. Jenkins, A. Kuzmich, T. A. B. Kennedy, *Nat. Phys.* **2010**, *6*, 894.
[40] B. Albrecht, P. Farrera, X. Fernandez-Gonzalvo, M. Cristiani, H. de Riedmatten, *Nat. Commun.* **2014**, *5*, 3376.
[41] S.-J. Yang, X.-J. Wang, X.-H. Bao, J.-W. Pan, *Nat. Photonics.* **2016**, *10*, 381.
[42] S. Z. W. M. J. Wang, T. Fei Ma, Y. Li, Y. Xie, H. L. Jiao, H. L. Liu, S. J. Li, H. Wang, *Quantum* **2023**, *7*, 903.
[43] L. Heller, P. Farrera, G. Heinze, H. de Riedmatten, *Phys. Rev. Lett.* **2020**, *124*, 210504.
[44] Y. Li, Y.-F. Wen, M.-J. Wang, C. Liu, H.-L. Liu, S.-J. Li, Z.-X. Xu, H. Wang, *Phys. Rev. A* **2022**, *106*, 022610.

© 2025 Wiley-VCH GmbH

25119044, 0, Downloaded from https://onlinelibrary.wiley.com/doi/10.1002/qute.202400480 by Shu-Jing Li - Shanxi University , Wiley Online Library on [12/02/2025]. See the Terms and Conditions (https://onlinelibrary.wiley.com/terms-and-conditions) on Wiley Online Library for rules of use; OA articles are governed by the applicable Creative Commons License